Applied Thermal Engineering 100 (2016) 999–1006

Contents lists available at ScienceDirect

Applied Thermal Engineering

journal homepage: www.elsevier.com/locate/apthermeng

Research Paper

CFD modelling of entropy generation in turbulent pipe flow: Effects of temperature difference and swirl intensity

Khalid M. Saqr *, Ali I. Shehata, Ahmed A. Taha, Mohamed M. Abo ElAzm

Mechanical Engineering Department, College of Engineering and Technology, Arab Academy for Science, Technology and Maritime Transport, P.O. Box 1029, Abu Quir, Alexandria, Egypt

HIGHLIGHTS

- The effects of swirl number and temperature difference on entropy generation in pipe flow were investigated.
- A CFD model was established and validated with experimental LDV measurements.
- The CFD model was used to simulate 77 cases representing $0 \le S_n \le 0.454$ and $0 \le \Delta T \le 60$
- Matlab was used to establish empirical correlations based on the CFD results.
- The empirical correlations predict entropy generation and Bejan number as functions of S_n and ΔT

GRAPHICAL ABSTRACT

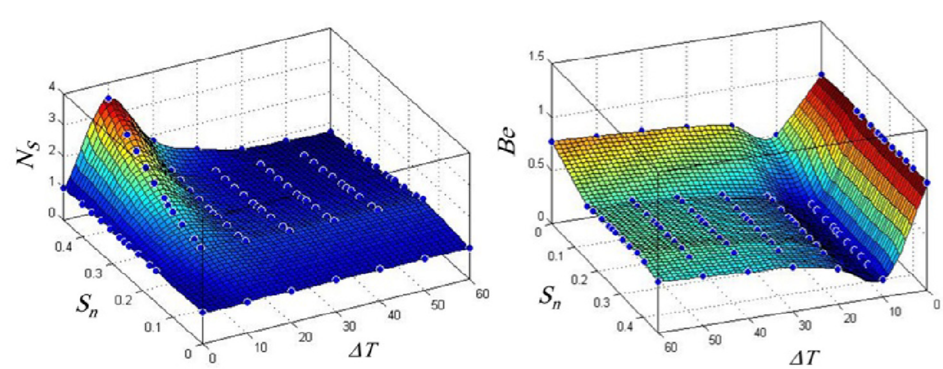

Surface plots for the nonlinear regression of the CFD results of entropy augmentation number (N_S) and Bejan number (Be) as functions of S_n and ΔT

ARTICLE INFO

Article history:
Received 20 June 2015
Accepted 5 February 2016
Available online 3 March 2016

Keywords:
Swirl flow
Entropy generation
Heat exchangers
Nonlinear regression
Matlab

ABSTRACT

This article extends the recent study by Saqr and Wahid *(Applied Thermal Engineering 70 (2014) 486–493)* on the criteria of heat transfer enhancement in swirl pipe flow based on the entropy generation minimization principle. The effects of wall–fluid temperature difference (ΔT) and swirl intensity (S_n) on entropy generation are considered in the present work. A Computational Fluid Dynamics (CFD) model of non-isothermal swirl pipe flow was developed, validated with established LDA measurements, and then used to study the Nusselt (Nu), entropy augmentation (N_s) and Bejan (Be) numbers in 77 different scenarios related to swirl-enhanced heat exchangers. Critical values of ΔT and S_n that correspond to unity N_s were identified. Then, based on the CFD results, two computer codes were developed in MATLAB software to correlate N_s and Be as functions of ΔT and S_n. These computer codes are openly provided in this article's appendix in order to contribute to the design and optimization tools of swirl-enhanced heat exchangers.

1. Introduction

Heat transfer enhancement (HTE) significantly increases the performance of heat exchangers, leading to reduced heat exchanger size and operating cost. HTE techniques can be classified into two categories: (1) active techniques which require external power source and (2) passive techniques which do not require external power

* Corresponding author. Tel.: +2035622586; fax: +2035622915.
E-mail address: k.saqr@aast.edu (K.M. Saqr).

http://dx.doi.org/10.1016/j.applthermaleng.2016.02.014
1359-4311/

Table 1
Summary of EGM studies of swirl heat transfer enhancement in pipe flows.

Reference	Method	Swirl generator	Reynolds number	EGM range
Yakut and Sahin [28]	Experimental	Coil wire inserts	$0.5\times10^4-3.5\times10^4$	$N_s<1$ for $\mathrm{Re}<1.3\times10^4$
Kurtbaş et al. [29]	Experimental	Propeller-type turbulators	$10^4-3\times10^4$	$N_s<1$ for $\mathrm{Re}<3\times10^4$
Kurtbaş et al. [30]	Experimental	Conical injector-type swirl generators	$10^4-3.5\times10^4$	$N_s<1$ for $\mathrm{Re}<2\times10^4$

source [1,2]. Swirl flow devices are one of the passive HTE techniques which are used to increase the overall rate of heat transfer by increasing the flow path and introduce an angular acceleration to the fluid flow [3–5]. The use of pipe inserts or inlet swirl generators is the most common method to achieve HTE by swirl flow [6]. During the past decade there have been numerous works which investigated the use of swirl-inducing pipe inserts, such as helical tapes [7,8], wires [9], and ribs [10]. The works on inlet swirl generators were relatively less than the former. Swirl flow can be imparted to the heat exchanger pipes by using tangential or semi-tangential inlets which forces the flow to develop a swirl velocity component at the inlet. The tangential velocity component achieves HTE by developing streamline curvature allowing the fluid to maintain a longer circumferential flow path, and by disturbing the thermal boundary layer via vortical structures [11–13]. While pipe inserts increase the pressure drop by reducing the pipes' hydraulic diameter, inlet swirl generators increase the required pumping power by increasing the friction and drag. Therefore, most of the works on HTE by swirl flow aimed at finding the optimum swirl intensity, at which HTE is achieved at the lowest budget of pressure loss.

A number of research investigated the effects of swirl on heat transfer enhancement in pipe flow by using the first law of thermodynamics. Experimental studies [14,15] showed that Nusselt number could be improved by 120%–150% due to swirl depending on the Reynolds number and swirl intensity. Computational studies [16] found that the Nusselt number could be improved by 50%–110%, while the friction factor increases much further by 90%–500% in swirl pipe flows under Reynolds number of 10^4 to 3×10^4. The general optimization goal of HTE studies is to reduce the size and cost of the heat exchanger while increasing its performance. For heat exchangers operating in power generation and HVAC applications, the role of heat exchanger in generating irreversibilities (i.e. entropy) in the system is crucial [17]. Entropy generation in the system as a whole is directly proportional to entropy generation within each component [18]. Hence, when a certain heat exchanger is modified or enhanced by any means, the entropy generation within the heat exchanger is affected, therefore entropy generation in the system is generally affected. This relation between entropy generation in heat exchangers and entropy generation in power generation and thermal equipment has been evidently proven in numerous studies [19–25]. According to Bejan [17], the thermodynamic design of any heat exchanger has two degrees of freedom which can be expressed by any pair of independent parameters such as $(\mathrm{St}, \Delta T)$, (Re, D_h) or $(\dot{m}, f)$ for any arbitrary heat transfer passage. Consequently, any method for HTE would radically affect the thermodynamic design of the heat exchanger. For example, any internal fins added to a passage of heat transfer would increase the overall heat transfer coefficient, and hence reduce the entropy generation due to heat transfer. However, the same enhancement would increase the friction factor, which will increase entropy generation due to viscous dissipation. Indeed there is a legacy of literature in the field of using the second law of thermodynamics and the entropy generation minimization method in optimizing heat exchangers of different types and for different objectives [26,27]. Many of such works focused on the validation and optimization of different HTE techniques. Several works attempted to investigate swirl HTE techniques by means of second law analysis. Bejan's entropy generation minimization (EGM) method was used to optimize swirl HTE methods such as coil turbulators [28] and propeller-type swirl generators [29–31]. Such methods are considered thermodynamically advantageous when N_s is less than unity. Table 1 summarizes the outcome of such works. These works have mainly investigated the effect of Reynolds number on entropy generation, while the effect of swirl number was not fully explored. The variation of swirl number in experimental works is difficult and expensive, since each swirl number would require a separate swirl generator. A swirl generator that can be altered to produce different swirl intensities was proposed in Reference 32, however it has not been utilized yet in investigating swirl flow instead of the fixed swirl number devices. Recently, Saqr and Wahid [33] studied the effect of swirl number on entropy generation in non-isothermal turbulent pipe flows using numerical simulation. The present work extends such recent study to include the effects of fluid–wall temperature difference in order to identify the criteria at which swirl minimizes entropy generation.

The literature review shows that there has been only a limited number of studies which reported the relationship between entropy generation in swirl pipe and swirl intensity. The work recently reported in [33] aimed at investigating such relationship at constant Reynolds number and fluid–wall temperature difference. The present article extends that recent study to include the effect of fluid–wall temperature difference, and define the criteria at which entropy generation could be minimized by the use of swirl. To the best of the authors' knowledge, such criteria have not been reported before. In the present work, heat transfer by convection and conduction in the steady Reynolds-averaged flow field were considered in the CFD model. The Reynolds stress term was closed using the realizable k-ε turbulence model which showed favourable predictions of swirl flow fields in previous studies [34,35]. The results of 77 CFD simulations were used to create two Matlab codes to predict the entropy augmentation number as well as the average Bejan number as functions of the swirl intensity and fluid–wall temperature difference. These codes are supplied openly with the present article.

2. Computational fluid dynamics model

2.1. Mathematical model

The flow considered in the present work is steady, incompressible, turbulent non-isothermal flow. The density ρ and viscosity μ of the fluid were set to 835 kg/m³ and 1.07×10^{-3} Pa·s to match the properties of the fluid used in the validation case [36]. The governing equation can be given in Einstein notation as

$$\textit{Continuity}: \frac{\partial}{\partial x_i}(\bar{u}_i)=0 \quad (1)$$

$$\text{RANS}: \frac{\partial}{\partial x_i}(\rho\bar{u}_i\bar{u}_j)=-\frac{\partial p}{\partial x_j}+\frac{\partial}{\partial x_j}\left[\mu\left(\frac{\partial\bar{u}_i}{\partial x_j}+\frac{\partial\bar{u}_j}{\partial x_i}-\frac{2}{3}\delta_{ij}\frac{\partial\bar{u}_j}{\partial x_i}\right)\right]+\frac{\partial}{\partial x_j}\left(-\rho\overline{u_i'u_j'}\right) \quad (2)$$

The Reynolds stress term is closed using the eddy viscosity assumption, given by

$$-\rho\overline{u_i'u_j'} = \mu_t\left(\frac{\partial \bar{u}_i}{\partial x_j}+\frac{\partial \bar{u}_j}{\partial x_i}\right)-\frac{2}{3}\delta_{ij}\left(\rho k+\mu_t\frac{\partial \bar{u}_k}{\partial x_k}\right) \tag{3}$$

where $\mu_t=\rho C_\mu \frac{k^2}{\varepsilon}$, and the turbulence kinetic energy k and its dissipation rate ε are given, respectively, by Shih's version of the realizable $k-\varepsilon$ model [37] as

$$\overline{u_i}\frac{\partial k}{\partial x_i} = \nu_t\left[\frac{\partial \overline{u_i}}{\partial x_j}+\frac{\partial \overline{u_j}}{\partial x_i}\right]\frac{\partial \overline{u_i}}{\partial x_j}+\frac{\partial}{\partial x_i}\left(\frac{\nu_t}{\sigma_k}\frac{\partial k}{\partial x_i}\right)-\varepsilon \tag{4}$$

$$\overline{u_i}\frac{\partial \varepsilon}{\partial x_i} = \frac{\partial}{\partial x_i}\left(\frac{\nu_t}{\sigma_\varepsilon}\frac{\partial \varepsilon}{\partial x_i}\right)+C_{\varepsilon 1}C_{\varepsilon 3}\frac{\varepsilon}{k}\nu_t\left[\frac{\partial \overline{u_i}}{\partial x_j}+\frac{\partial \overline{u_j}}{\partial x_i}\right]\frac{\partial \overline{u_i}}{\partial x_j} + C_1 S_\varepsilon - C_2\frac{\varepsilon^2}{k+\sqrt{\nu\varepsilon}} \tag{5}$$

where the model constants are given by $C_{\varepsilon 1}=1.44$, $C_{\varepsilon 2}=1.92$, $C_1=\max\left(0.43,\frac{\eta}{\eta+5}\right)$, and $C_2=1.9$. C_μ is not a constant and is computed from

$$C_\mu = \frac{1}{A_0 + A_s U^* \dfrac{k}{\varepsilon}} \tag{6}$$

where $A_0=4.0$; $U^*=\sqrt{S_{ij}S_{ij}+\Omega_{ij}\Omega_{ij}}$, $A_s=\sqrt{6}\cos\left(\frac{1}{3}\arccos\left(\sqrt{6}W\right)\right)$, $W=\frac{\sqrt{8}S_{ij}S_{jk}S_{ki}}{S^3}$, and the vorticity tensor is given by $\Omega_{ij}=\frac{1}{2}\left(\frac{\partial \bar{u}_i}{\partial x_j}-\frac{\partial \bar{u}_j}{\partial x_i}\right)$, where the Einstein summation convention in generalized two-dimensional axisymmetric coordinates is given by $\frac{\partial}{\partial x_i}=\frac{\partial}{\partial x}+\frac{\partial}{\partial r}+\frac{1}{r}$.

In fact, this version of the realizable $k-\varepsilon$ turbulence model has shown a very good performance in predicting flows with streamline curvature, such as swirl flows. The formulation of a mean-flow dependent C_μ, as given by Equation (6), ensures that the model only takes the effect of positive normal stresses on the mean flow as well as satisfying Schwarz inequality condition for shear stress. The performance of such model with swirl and vortex flow has been tested in a number of recent studies such as in [32,34,35,38].

The energy equation for steady-state convective flow, excluding radiation heat transfer, is given as

$$\rho\frac{\partial}{\partial x_i}\cdot(\bar{u}_i(E+p)) = \frac{\partial}{\partial x_i}\cdot\left(k_{eff}\nabla T - h\psi + \bar{\bar{\tau}}\bar{u}_i\right) \tag{7}$$

where $E=h-\frac{p}{\rho}+\frac{\bar{u}_i^2}{2}$, $\bar{\bar{\tau}}=\mu[2S-\frac{2}{3}\delta\nabla\cdot\bar{u}_i]$ and $S=\frac{1}{2}(\nabla\cdot\bar{u}_i+\nabla\cdot\bar{u}_i^T)$.

Considering the heat and mass irreversibilities on the flow in hand, the local entropy generation can be expressed as [39,40]

$$\dot{S}_{gen} = \frac{k}{T^2}\left(\frac{\partial T}{\partial x_j}\right)^2 + \frac{\mu}{T}\frac{\partial \bar{u}_i}{\partial x_j}\left(\frac{\partial \bar{u}_i}{\partial x_j}+\frac{\partial \bar{u}_j}{\partial x_j}\right) \tag{8}$$

where the first and second terms on the RHS refer to entropy generation due to heat transfer $\dot{S}_{ht}$ and viscous dissipation $\dot{S}_V$, respectively. Swirl number is the ratio between axial flux of tangential momentum and axial thrust, and can be calculated as [41]

$$S_n = \frac{\int_0^R u_x u_\theta r dr}{R\int_0^R u_x^2 r dr} \tag{9}$$

2.2. Numerical solution details

The computational domain used in the present work was similar to the one used in Reference 33. A two dimensional axisymmetric flow domain with a length of 1100 mm and a radius of 50 mm was generated in GAMBIT software. The geometry and computational domains are shown in Fig. 1. A non-uniform grid containing 86,625

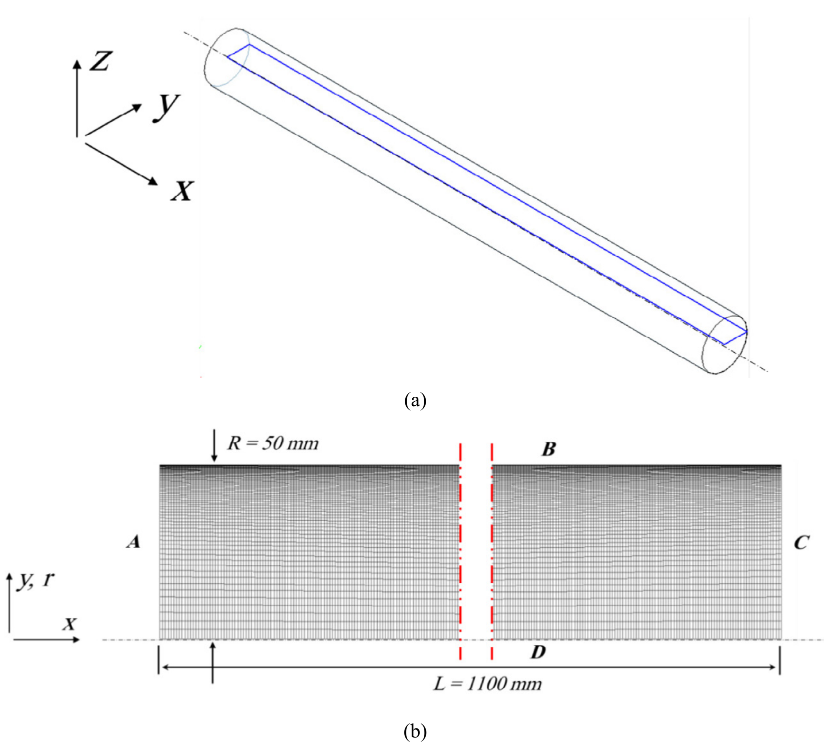

Fig. 1. Schematic of the computational geometry and domain showing (a) plane of cylindrical symmetry relative to the pipe and (b) two-dimensional axisymmetric grid. A, B, C and D denote the location of boundary conditions of the domain.

Table 2
Type and location of boundary conditions used in the CFD model.

Boundary condition	A	B	C	D
Velocity	Inlet velocity profiles	No-slip	None	Axis (rotational symmetry)
Pressure	None	None	Outlet pressure	
Temperature	Constant temperature (fluid)	Constant temperature (wall)	None	

quadrilateral cells was used after ensuring that it provides grid-independent solution, as shown in Reference 33. Smaller cells were positioned near to the pipe wall in order to capture the swirl decay behaviour, as shown in Fig. 1b. The general purpose CFD code FLUENT [42] was used to solve the governing equations of the problem on the computational domain. The pressure-based solver which utilizes the Semi-implicit Method for Pressure Linked Equations (SIMPLE) [43] was selected. Spatial discretization was achieved using a second order upwind scheme [44]. In this approach, a higher-order of accuracy is achieved at cell faces through a Taylor series expansion of the cell-centred solution about the cell centroid. A logarithmic wall function of the standard type [45] was used with the realizable k-ε turbulence model to resolve the near-wall velocity field. Moreover, implicit relaxation factors were used to help the solution convergence and stability. The types of boundary condition set to the domain are shown in Table 2. Each case required approximately 18×10^3 iterations in order to converge.

2.2.1. Boundary conditions

The velocity profiles for the axial and tangential velocity components were adopted from Reference 36. The tangential velocity profile was linearly scaled to achieve the swirl number range $0 \le S_n \le 0.454$ with an approximately average increment of 0.03. The fluid–wall temperature difference was changed within the range of $0 \le \Delta T \le 60$ with an increment of 10 degrees. Therefore, the number of simulations was 77 cases representing different scenarios of swirl intensity and temperature difference.

2.2.2. Treatment of near-wall flow

The logarithmic law of the wall was used to predict the near-wall velocity as proposed in Reference 45. Such law expresses the mean near-wall velocity as

$$U^* = \frac{1}{k}\ln(Ey^*) \tag{10}$$

and

$$y^* \equiv \frac{1}{\mu}\rho C_\mu^{\frac{1}{4}} k_p^{\frac{1}{2}} y_p \tag{11}$$

where k is von Kármán constant (0.4187), E is empirical constant (9.793), k_p is turbulence kinetic energy at point p, and y_p is the distance between point p and the wall. The law in Equation (10) is valid for $30 < y^* < 300$. In all the simulation cases presented here, y^* was maintained in between 40 and 70 to ensure the applicability of the log. law of the wall.

2.3. Model validation

The CFD model used in the present study was validated against established LDV measurements from Reference 36. The results of the validation are shown in Fig. 2 [33]. The CFD model is shown to successfully predict the axial and tangential velocity profiles at different locations. Shih's realizable $k-\varepsilon$ model has a very good record

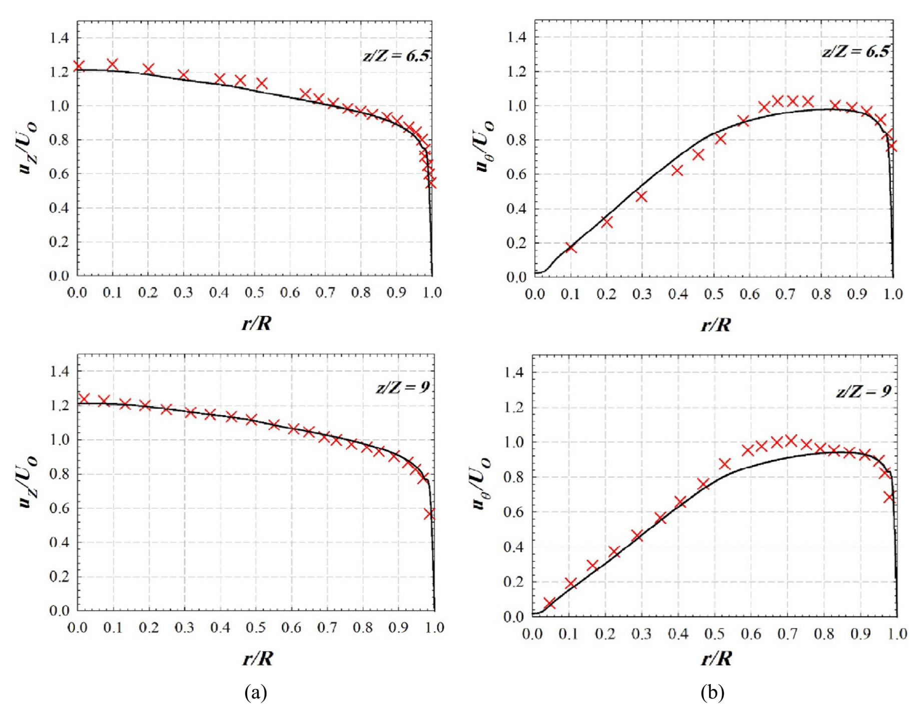

Fig. 2. Validation of the CFD model, the top and bottom rows show normalized radial profiles of (a) axial and (b) tanegnatial velocity, respectively, at two axial distances (z/Z = 6.5, 9). Cross marks indicate LDV measurements from Reference 32 and lines indicate CFD results of the present model.

of predicting flow fields characterized with swirl and high streamline curvature in numerous studies covering wide range of applications, Reynolds and swirl numbers [32,34,35,46–52]. Nevertheless, it can be noted that the predictions of the tangential velocity profiles are less accurate than such of the axial velocity. This can be justified by the limitation of inherited anisotropy in the model due to the eddy viscosity assumption, as it appears in Equation (3).

3. Results and discussion

The results presented in this section are based on 77 simulation cases. The values of dimensionless numbers such as Bejan, Nusselt and entropy augmentation numbers were calculated for each case as an area-average value. Since the independent (i.e. control) parameters are two, S_n and ΔT, planar contour plots were used to investigate the results in order to enable the analysis of the effects of both independent parameters on one dependent variable at the same time. The results of individual cases, as such discussed in [33], were not presented in details here to avoid redundancy.

3.1. Effects of ΔT and S_n on Nusselt number

Fig. 3 shows a contour map for the Nusselt number as it changes due to the variation of ΔT and S_n. It can be seen that the Nusselt number is directly proportional to both independent variables. However, the slope of the isolines shown on the map indicates that the increase of ΔT has a greater effect on *Nu* than the increase of S_n. The results here agree with the reports of Nusselt number in various swirl-enhanced heat transfer equipment as in [7,53,54].

3.2. Effects of ΔT and S_n on Bejan number

Bejan number is the ratio between thermal and total entropy generation rates. Fig. 4 shows a contour map for *Be* as function of ΔT and S_n. The map can be easily characterized to three zones based on the trend of *Be* values with respect to ΔT and S_n, as denoted by the dashed lines. The first zone $(0.155 > S_n)$ is characterized by moderate *Be* $(0.3 < Be < 0.75)$ with approximately equal response of

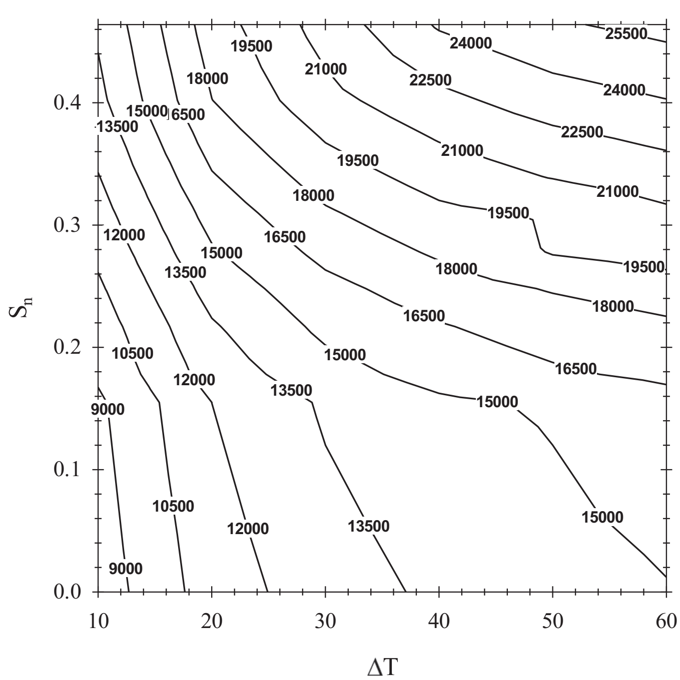

Fig. 3. Contour map of *Nu* as a function of ΔT and S_n.

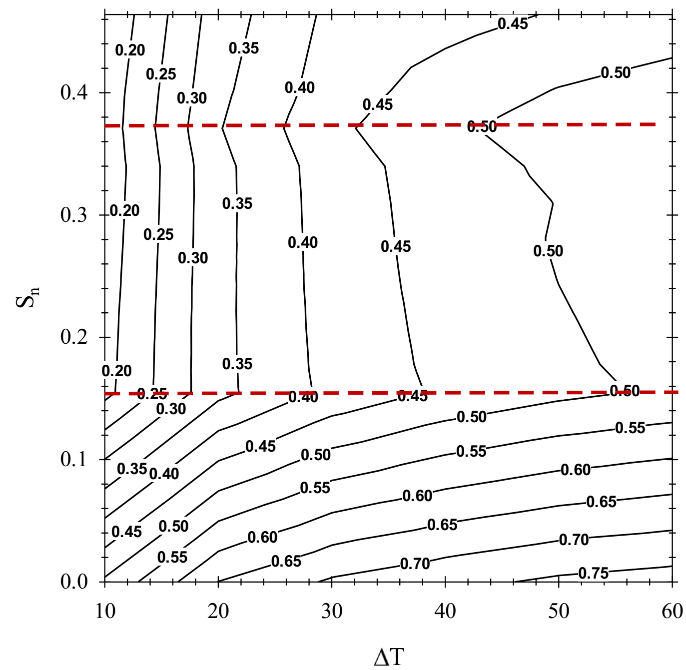

Fig. 4. Contours of *Be* as a function of S_n and ΔT.

Be to the change in ΔT and S_n. However, the second zone $(0.155 < S_n < 0.367)$ is characterized by a very limited effect of S_n on *Be* compared to ΔT at $(30 > \Delta T$. At higher temperature differences $(30 < \Delta T < 60)$, *Be* trend is opposite to such of the first zone. The values of *Be* in the second zone show that the flow became dominated by viscous entropy generation $(0.5 > Be$ The case is similar in the third zone $(0.367 < S_n < 0.454)$ where *Be* contours return to similar trend of such of the first zone, but still demonstrates relatively higher dependence on ΔT than such on S_n.

3.3. Effects of ΔT and S_n on entropy augmentation number

The entropy augmentation number N_s represents the ratio between entropy generation due to swirl and entropy generation in zero-swirl pipe flows. It characterizes the second law efficiency of the flow under investigation. Fig. 5 shows contour maps for N_s as function of ΔT and S_n. Swirl is evidently shown to minimize entropy generation only at high ΔT and S_n $(30 < \Delta T$ and $0.3 < S_n)$. This limit is depicted by the unity N_s contour line in the upper right corner of the figure. These conditions correspond to the highest values of *Nu* as well as *Be* values which correspond to 50% heat transfer irreversibilities. It can also be noticed that the lowest entropy generation rate is associated with higher values of Nusselt number.

3.4. The interaction between entropy generation mechanisms in swirl flow

In pipe flow associated with heat transfer, entropy generates in the system due to two mechanisms which are represented as $\dot{S}_{ht}$ and $\dot{S}_V$ [55]. Swirl velocity component increases the viscous dissipation due to the streamline curvature effects [56], hence increasing $\dot{S}_V$. On the other hand, the swirl velocity improves mixing and enhances the overall heat transfer coefficient, hence reducing $\dot{S}_{ht}$. Therefore, the swirl velocity components, in addition to the fluid–wall temperature difference, affect both mechanisms of entropy generation. It was reported in that in thermodynamically disadvantageous situations $(N_s > 1)$, the flow is dominated by viscous irreversibilities. On the other hand, at situations where $(N_s < 1)$, both

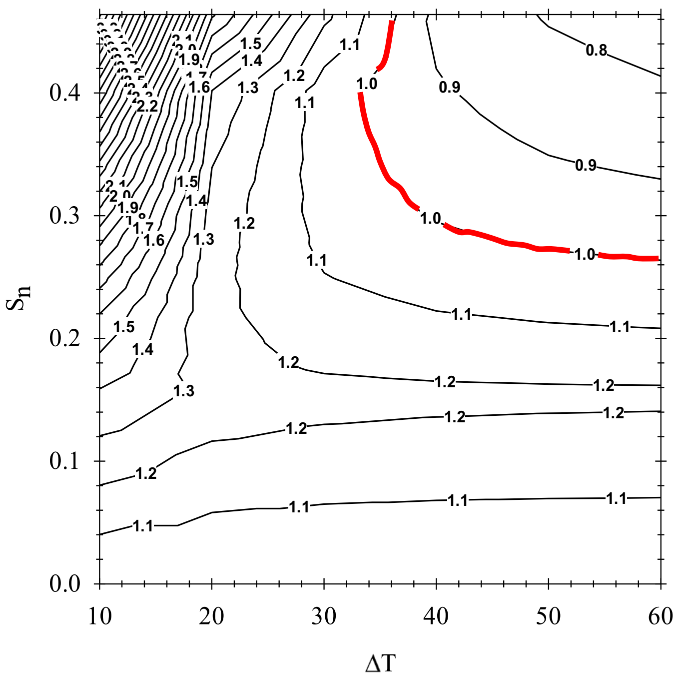

Fig. 5. Contours of entropy augmentation number N_s as a function of S_n and ΔT.

thermal and viscous irreversibilities constitute comparable roles in the entropy generation mechanism of the flow. The investigation of the effects of ΔT in the present work confirmed these phenomena. In Fig. 6a and b, each symbol mark represents a CFD case. In Fig. 6a it is clearly shown that thermodynamically advantageous conditions can only occur when *Be* is around the value of 0.5. This is further confirmed by Fig. 6b where the ratio between viscous and thermal irreversibilities was plot against the swirl number for different ΔT values. For the cases where $N_s < 1$, the ratio between two entropy generation mechanisms approximately is in the range of 0.9 to 1.4, which indicates comparable – or competing – roles of both mechanisms.

3.5. Matlab codes for entropy generation calculations

The computer package Matlab® was used to conduct a three dimensional nonlinear regression of the CFD results to provide a way for calculating *Be* and N_s as functions of ΔT and S_n. The nonlinear regression functions and their corresponding codes are detailed in Table 3. The correlations resulting from the nonlinear regression were used to plot the datasets in three dimensions giving the surface plots shown in Fig. 7. The surface fitting tool box was used for the nonlinear regression. It is evidently shown that both functions are highly nonlinear, especially at low and high values of ΔT for N_s and *Be*, respectively. The codes can easily be used to find critical values for N_s and *Be* by nonlinear interpolation.

4. Conclusions

CFD simulations of the non-isothermal turbulent pipe flow with different levels of swirl have been performed to investigate the effect of swirl level and wall–fluid temperature difference on heat transfer and entropy generation. It was found that the relationship between entropy generation, swirl number and temperature difference is nonlinear. Swirl could achieve entropy generation minimization only at high ΔT and S_n ($30 < \Delta T$ and $0.3 < S_n$). These conditions correspond to *Be* values around 0.5, and the highest values

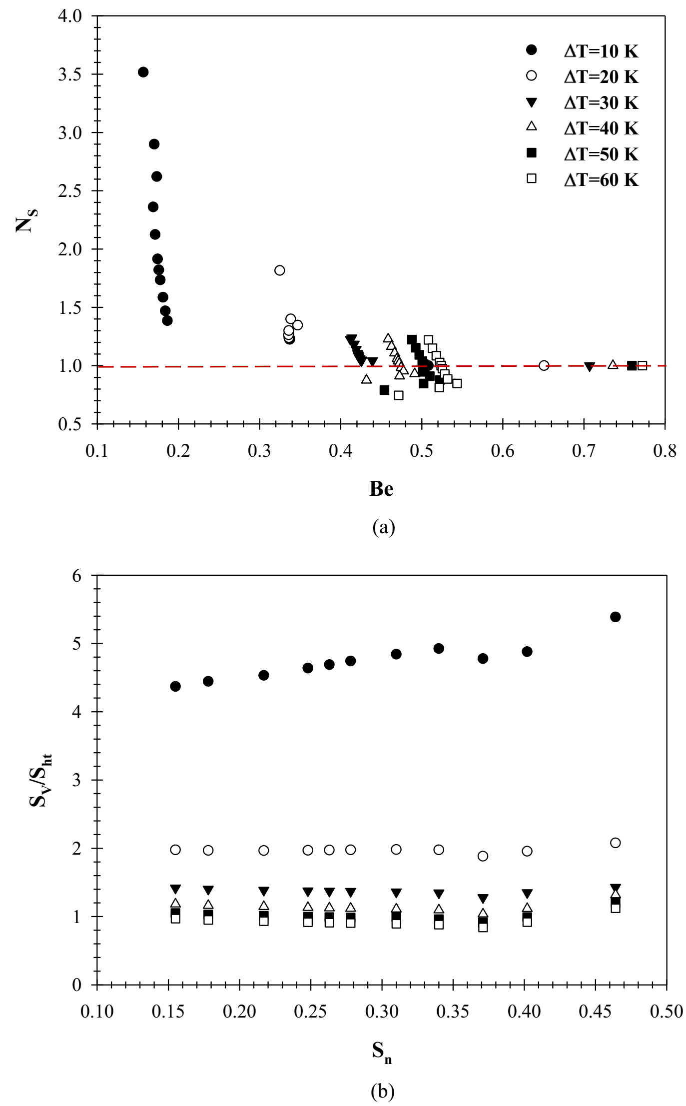

Fig. 6. (a) Entropy augmentation number as a function of Bejan number for different values of ΔT. (b) The ratio between viscous and thermal irreversibilities as a function of swirl number for different values of ΔT.
Legend of 6(a) is similar to 6(b).

of *Nu*. Computer codes were formulated based on the CFD results to provide nonlinear regression for both *Be* and N_s. The codes have two objectives: to provide a predictive tool for second law optimization of swirl pipe flow and to enable the readers to reproduce the

Table 3
Code parameters for *Be* and N_s nonlinear regression.

Data name	Regression function	Codes	
		File name	Function
N_s	Interpolant cubic	EntropyAugment.m	Dataset for N_s
		creatsurfacefit4.m	Function file for the raw N_s data
		creatsurfacefit3.m	Function file for the regression data of N_s
Be	Interpolant cubic	Bejan.m	Dataset for *Be*
		createsurfacefit5.m	Function file for the raw *Be* data
		createsurfacefit6.m	Function file for the regression data of *Be*

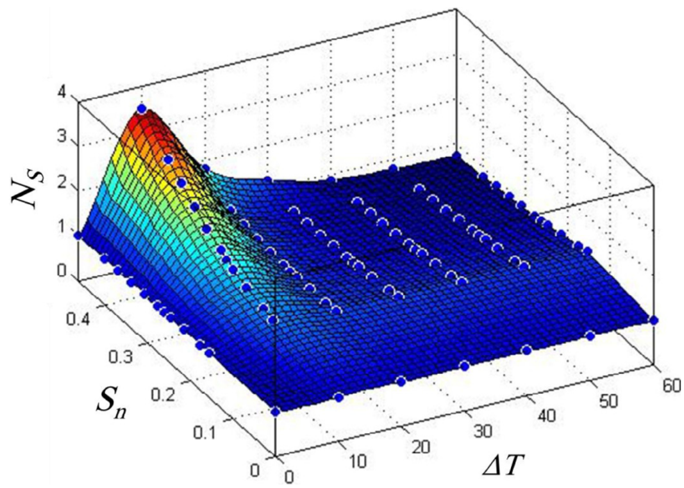

(a)

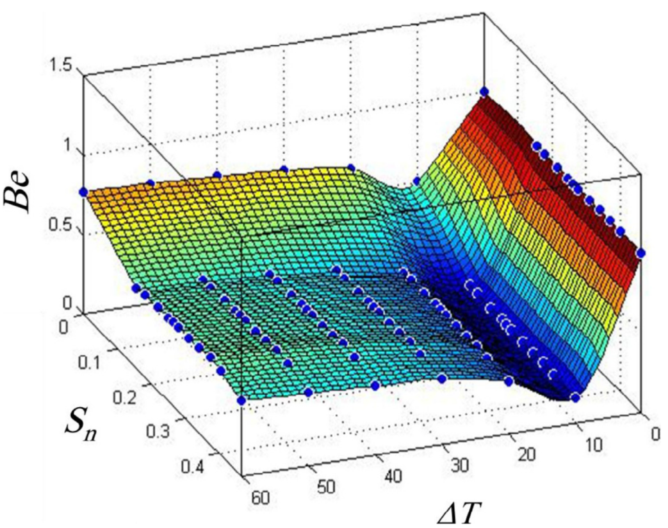

(b)

Fig. 7. Surface plots for the nonlinear regression of the CFD results of (a) entropy augmentation number and (b) Bejan number, as functions of S_n and ΔT.

results of the present work without the need to perform CFD simulations again.

Appendix: Spplementary material

Supplementary data to this article can be found online at doi:10.1016/j.applthermaleng.2016.02.014.

Nomenclature

Latin symbols

$\bar{u}$ Reynolds averaged velocity vector ($m \cdot s^{-1}$)
p Pressure ($kg \cdot m^{-1} \cdot s^{-2}$)
u' Fluctuating velocity vector ($m \cdot s^{-1}$)
u_x Axial velocity component ($m \cdot s^{-1}$)
u_θ Tangential velocity component ($m \cdot s^{-1}$)
k Turbulence kinetic energy ($m^2 \cdot s^{-2}$)
h Enthalpy ($kg \cdot m^2 \cdot s^{-2}$)
T Temperature (k)
S_n Swirl number (dimensionless)
St Stanton number (dimensionless)
Re Reynolds number (dimensionless)
Be Bejan number (dimensionless)
Nu Nusselt number (dimensionless)
N_s Entropy augmentation number (dimensionless)
$\dot{S}_{ht}$ Entropy generation rate due to heat transfer irreversibilities ($W \cdot m^{-3} \cdot K^{-1}$)
$\dot{S}_V$ Entropy generation rate due to viscous irreversibilities ($W \cdot m^{-3} \cdot K^{-1}$)
$\dot{S}_{gen}$ Total rate of entropy generation ($W \cdot m^{-3} \cdot K^{-1}$)
S_{ijk} Mean rate of strain tensor (s^{-1})
ΔT Temperature difference (K)
D_h Hydraulic diameter (m)
f Friction factor (dimensionless)

Greek symbols

ρ Density ($kg \cdot m^{-3}$)
μ_t Turbulent viscosity ($kg \cdot m^{-1} \cdot s^{-1}$)
ε Dissipation rate ($m^2 \cdot s^{-3}$)
Ω_{ij} Vorticity tensor (s^{-1})
ν_t Kinematic turbulent viscosity ($m^{-2} \cdot s^{-1}$)
δ_{ij} Kronecker's delta operator

References

[1] E.M. Smith, Thermal Design of Heat Exchangers: A Numerical Approach: Direct Sizing and Stepwise Rating, Wiley, 1997.
[2] S. Liu, M. Sakr, A comprehensive review on passive heat transfer enhancements in pipe exchangers, Renew. Sustain. Energy Rev. 19 (2013) 64–81.
[3] F. Kreith, R. Manglik, M. Bohn, Principles of Heat Transfer, Cengage Learning, 2010.
[4] T. Kuehn, R. Goldstein, An experimental and theoretical study of natural convection in the annulus between horizontal concentric cylinders, J. Fluid Mech. 74 (1976) 695–719.
[5] S. de Parias Neto, P. Legentilhomme, J. Legrand, Finite-element simulation of laminar swirling decaying flow induced by means of a tangential inlet in an annulus, Comput. Methods Appl. Mech. Eng. 165 (1998) 189–213.
[6] Y.A. Kuzma-Kichta, Heat transfer intensification: a review, Heat Transf. Res. 31 (2000) 146–158.
[7] P. Sivashanmugam, S. Suresh, Experimental studies on heat transfer and friction factor characteristics of laminar flow through a circular tube fitted with helical screw-tape inserts, Appl. Therm. Eng. 26 (2006) 1990–1997.
[8] R.M. Manglik, A.E. Bergles, Swirl flow heat transfer and pressure drop with twisted-tape inserts, Adv. Heat Transfer 36 (2003) 183–266.
[9] D.L. Youchison, C.H. Cadden, D.E. Driemeyer, G.W. Wille, Evaluation of helical wire inserts for CHF enhancement, in: Proceedings – Symposium on Fusion Engineering, 1999, pp. 119–122.
[10] K. Nanan, M. Pimsarn, C. Thianpong, S. Eiamsa-Ard, Heat transfer enhancement by helical screw tape coupled with rib turbulators, J. Mech. Sci. Technol. 28 (2014) 4771–4779.
[11] F. Chang, V. Dhir, Mechanisms of heat transfer enhancement and slow decay of swirl in tubes using tangential injection, Int. J. Heat Fluid Fl. 16 (1995) 78–87.
[12] K. Yajnik, M. Subbaiah, Experiments on swirling turbulent flows. Part 1. Similarity in swirling flows, J. Fluid Mech. 60 (1973) 665–687.
[13] O. Kitoh, Experimental study of turbulent swirling flow in a straight pipe, J. Fluid Mech. 225 (1991) 445–479.
[14] A. Durmuş, A. Durmuş, M. Esen, Investigation of heat transfer and pressure drop in a concentric heat exchanger with snail entrance, Appl. Therm. Eng. 22 (2002) 321–332.
[15] M. Yilmaz, O. Comakli, S. Yapici, O.N. Sara, Heat transfer and friction characteristics in decaying swirl flow generated by different radial guide vane swirl generators, Energy Convers. Manag. 44 (2003) 283–300.
[16] M. Ahmadvand, A.F. Najafi, S. Shahidinejad, An experimental study and CFD analysis towards heat transfer and fluid flow characteristics of decaying swirl pipe flow generated by axial vanes, Meccanica 45 (2010) 111–129.
[17] A. Bejan, The thermodynamic design of heat and mass transfer processes and devices, Int. J. Heat Fluid Fl. 8 (1987) 258–276.
[18] A. Bejan, Second-law analysis in heat transfer and thermal design, Adv. Heat Transfer 15 (1982) 1–58.
[19] R.T. Ogulata, F. Doba, Experiments and entropy generation minimization analysis of a cross-flow heat exchanger, Int. J. Heat Mass Transf. 41 (1998) 373–381.
[20] J.C. Ordóñez, A. Bejan, Entropy generation minimization in parallel-plates counterflow heat exchangers, Int. J. Energy Res. 24 (2000) 843–864.
[21] J.V.C. Vargas, A. Bejan, Thermodynamic optimization of finned crossflow heat exchangers for aircraft environmental control systems, Int. J. Heat Fluid Fl. 22 (2001) 657–665.
[22] V. Zimparov, Energy conservation through heat transfer enhancement techniques, Int. J. Energy Res. 26 (2002) 675–696.

[23] P.K. Singh, K.B. Anoop, T. Sundararajan, S.K. Das, Entropy generation due to flow and heat transfer in nanofluids, Int. J. Heat Mass Transf. 53 (2010) 4757–4767.
[24] P. Ahmadi, H. Hajabdollahi, I. Dincer, Cost and entropy generation minimization of a cross-flow plate fin heat exchanger using multi-objective genetic algorithm, J. Heat Transfer 133 (2011) 021801.
[25] Q. Chen, J. Wu, M. Wang, N. Pan, Z. Guo, A comparison of optimization theories for energy conservation in heat exchanger groups, Chin. Phys Lett 56 (2011) 449–454.
[26] S. Sieniutycz, Thermodynamic limits on production or consumption of mechanical energy in practical and industrial systems, Prog. Energ. Combust. 29 (2003) 193–246.
[27] A. Bejan, Entropy generation minimization: the new thermodynamics of finite-size devices and finite-time processes, J. Appl. Phys. 79 (1996) 1191–1218.
[28] K. Yakut, B. Sahin, The effects of vortex characteristics on performance of coiled wire turbulators used for heat transfer augmentation, Appl. Therm. Eng. 24 (2004) 2427–2438.
[29] I. Kurtbaş, A. Durmuş, H. Eren, E. Turgut, Effect of propeller type swirl generators on the entropy generation and efficiency of heat exchangers, Int. J. Therm. Sci. 46 (2007) 300–307.
[30] I. Kurtbaş, F. Gülçimen, A. Klçarslan, M. Kaya, Effect of swirl generator inserted into a tube on exergy transfer: decaying flow, Exp. Heat Transfer 27 (2014) 472–487.
[31] T. Bali, B.A. Sarac, Exergy analysis of heat transfer in a turbulent pipe flow by a decaying swirl generator, Int. J. Exergy 5 (2008) 64–77.
[32] Y.A. Eldrainy, K.M. Saqr, H.S. Aly, M.N.M. Jaafar, CFD insight of the flow dynamics in a novel swirler for gas turbine combustors, Int. Commun. Heat Mass 36 (2009) 936–941.
[33] K.M. Saqr, M.A. Wahid, Effects of swirl intensity on heat transfer and entropy generation in turbulent decaying swirl flow, Appl. Therm. Eng. 70 (2014) 486–493.
[34] B. Rohani, K.M. Saqr, Effects of hydrogen addition on the structure and pollutant emissions of a turbulent unconfined swirling flame, Int. Commun. Heat Mass 39 (2012) 681–688.
[35] Y.A. Eldrainy, K.M. Saqr, H.S. Aly, T.M. Lazim, M.N.M. Jaafar, Large eddy simulation and preliminary modeling of the flow downstream a variable geometry swirler for gas turbine combustors, Int. Commun. Heat Mass 38 (2011) 1104–1109.
[36] G. Rocklage-Marliani, M. Schmidts, V. Vasanta Ram, Three-dimensional laser-doppler velocimeter measurements in swirling turbulent pipe flow, Flow Turbul. Combust. 70 (2003) 43–67.
[37] T.-H. Shih, W.W. Liou, A. Shabbir, Z. Yang, J. Zhu, A new k-ε eddy-viscosity model for high Reynolds number turbulent flows – model development and validation, Comput. Fluids 24 (1995) 227–238.
[38] Y.A.E. Drainy, K.M. Saqr, H.S. Aly, M.N. Mohd, M. Jaafar, CFD analysis of incompressible turbulent swirling flow through zanker plate, Eng. Appl. Comp. Fluid 3 (2009) 562–572.
[39] S. Chen, Z. Liu, J. Liu, J. Li, L. Wang, C. Zheng, Analysis of entropy generation in hydrogen-enriched ultra-lean counter-flow methane-air non-premixed combustion, Int. J. Hydrogen Energy 35 (2010) 12491–12501.
[40] B.S. Yilbas, S.Z. Shuja, M.O. Budair, Second law analysis of a swirling flow in a circular duct with restriction, Int. J. Heat Mass Transf. 42 (1999) 4027–4041.
[41] K.M. Saqr, H.I. Kassem, H.S. Aly, M.A. Wahid, Computational study of decaying annular vortex flow using the R ε/k-ε turbulence model, Appl. Math. Model. 36 (2012) 4652–4664.
[42] ANSYS, FLUENT 6.3 User Guide in, ANSYS, Inc., 2006.
[43] S.V. Patankar, D.B. Spalding, A calculation procedure for heat, mass and momentum transfer in three-dimensional parabolic flows, Int. J. Heat Mass Transf. 15 (1972) 1787–1806.
[44] B. Timothy, J. Dennis, The design and application of upwind schemes on unstructured meshes, in: 27th Aerospace Sciences Meeting, American Institute of Aeronautics and Astronautics, 1989.
[45] B.E. Launder, D.B. Spalding, The numerical computation of turbulent flows, Comput. Methods Appl. Mech. Eng. 3 (1974) 269–289.
[46] Z. Chen, Z. Li, J. Jing, L. Xu, L. Chen, S. Wu, et al., Numerical simulation of gas-particle two phase flow field for swirl burner, Jixie Gongcheng Xuebao/J. Mech. Eng. 45 (2009) 305–310.
[47] H.F. Guo, Z.Y. Chen, C.W. Yu, 3D numerical simulation of compressible swirling flow induced by means of tangential inlets, Int. J. Numer. Methods Fluids 59 (2009) 1285–1298.
[48] R. Hreiz, C. Gentric, N. Midoux, Numerical investigation of swirling flow in cylindrical cyclones, Chem. Eng. Res. Design 89 (2011) 2521–2539.
[49] A.K. Sharma, C. Bhattacharya, S. Sen, A. Mukhopadhyay, A. Datta, Analysis of different radiation models in a swirl stabilized combustor, in: ASME 2014 Gas Turbine India Conference, GTINDIA 2014, 2014.
[50] M. Usman, S. Malik, M. Rafique, Probability density function computations of a strongly swirling flame, in: Proceedings of 2012 9th International Bhurban Conference on Applied Sciences and Technology, IBCAST 2012, 2012, pp. 283–290.
[51] C.H. Cho, G.M. Baek, C.H. Sohn, J.H. Cho, H.S. Kim, A numerical approach to reduction of NOx emission from swirl premix burner in a gas turbine combustor, Appl. Therm. Eng. 59 (2013) 454–463.
[52] M. Miltner, C. Jordan, M. Harasek, CFD simulation of straight and slightly swirling turbulent free jets using different RANS-turbulence models, Appl. Therm. Eng. 89 (2015) 1117–1126.
[53] J. Wang, W. Liu, Z. Liu, The application of exergy destruction minimization in convective heat transfer optimization, Appl. Therm. Eng. 88 (2015) 384–390.
[54] Z. Zhao, D.W. Yuen, C.W. Leung, T.T. Wong, Thermal performance of a premixed impinging circular flame jet array with induced-swirl, Appl. Therm. Eng. 29 (2009) 159–166.
[55] A. Bejan, A study of entropy generation in fundamental convective heat transfer, J. Heat Transfer 101 (1979) 718–725.
[56] R.R. Parchen, W. Steenbergen, J. Voskamp, An experimental and numerical study of turbulent swirling pipe flows, J. Fluid. Eng.-T. ASME 120 (1998) 54–61.